

Structure and diffusion in amorphous aluminium silicate: A molecular dynamics computer simulation

Anke Winkler¹⁾, Jürgen Horbach¹⁾, Walter Kob²⁾, and Kurt Binder¹⁾

¹⁾*Institut für Physik, Johannes Gutenberg-Universität,
D-55099 Mainz, Staudinger Weg 7, Germany*

²⁾*Laboratoire des Verres, Université Montpellier II,
F-34095 Montpellier, France*

Abstract

The amorphous aluminium silicate $(\text{Al}_2\text{O}_3)_2(\text{SiO}_2)$ [AS2] is investigated by means of large scale molecular dynamics computer simulations. We consider fully equilibrated melts in the temperature range $6100 \text{ K} \geq T \geq 2300 \text{ K}$ as well as glass configurations that were obtained from cooling runs from $T = 2300 \text{ K}$ to 300 K with a cooling rate of about 10^{12} K/s . Already at temperatures as high as 4000 K , most of the Al and Si atoms are four-fold coordinated by oxygen atoms. Thus, the structure of AS2 is that of a disordered tetrahedral network. The packing of AlO_4 tetrahedra is very different from that of SiO_4 tetrahedra in that Al is involved with a relatively high probability in small-membered rings and in triclusters in which an O atom is surrounded by four cations. We find as typical configurations two-membered rings with two Al atoms in which the shared O atoms form a tricluster. On larger length scales, the system shows a microphase separation in which the Al-rich network structure percolates through the SiO_2 network. The latter structure gives rise to a prepeak in the static structure factor at a wavenumber $q = 0.5 \text{ \AA}^{-1}$. The comparison of experimental X-ray data with the results from the simulation shows a good agreement for the structure function. The diffusion dynamics in AS2 is found to be much faster than in SiO_2 . We show that the self-diffusion constants for O and Al are very similar and that they are by a factor of 2–3 larger than the one for Si.

1 Introduction

Amorphous mixtures of SiO_2 with other oxides such as Na_2O or Al_2O_3 are of fundamental interest in geosciences [1] and glass technology [2]. These systems exhibit many of the physical phenomena that one encounters in multicomponent melts: E.g. in sodium silicates the sodium ions are much more mobile than the silicon and oxygen atoms which leads to the property of ion conductance at low temperature [3]. Or in the mixture $\text{SiO}_2\text{--Al}_2\text{O}_3$ a miscibility gap emerges which is already present at temperatures slightly below 2000 K [4, 5, 6]. Some recent computer simulations have shown that in order to understand these properties of silicate melts one needs an accurate knowledge of their microscopic structure [7]: For instance, pure amorphous silica forms a network of corner-shared SiO_4 tetrahedra and it is known from Molecular Dynamics (MD) computer simulations that diffusive motions are dominated by the existence of defects such as SiO_3 and SiO_5 units in the network (see, e.g., Refs. [8, 9]). Another example is the sodium diffusion in sodium silicates: Molecular dynamics simulation studies have demonstrated that the sodium diffusion can be understood in terms of a motion through a channel network which is embedded in the SiO_2 matrix [10, 11, 12, 13], and that the characteristic length scale of this channel network is directly related to a prepeak in the static structure factor at $q = 0.95 \text{ \AA}^{-1}$ [14, 15] the existence of which has been verified in a recent neutron scattering experiment [16]. Despite this progress in our understanding of the microscopic structure of these materials, many properties of silicates are still understood only poorly. E.g. the influence of a second network former, such as Al, on the structural and dynamical properties, or on the phase diagram are still not very clear. Therefore, the goal of the present paper is to shed some light on this matter.

Aluminium silicate glasses have been investigated by means of different experimental techniques such as Nuclear Magnetic Resonance (NMR) [17, 18, 19, 20, 21, 22, 23], IR and Raman spectroscopy, and X-ray scattering [24, 25, 26]. One of the main issues in these experiments has been the analysis of the local structure around the aluminium atoms. This is of special importance for understanding the chemical ordering in aluminium silicates since in principle the Al^{3+} ions do need a different environment of O^{2-} ions than the Si^{4+} ions in order to provide local charge neutrality. Noteworthy are two peculiarities that have been found in the experimental studies that distinguish the local oxygen environment of an Al from that of a Si atom: In systems with a high Al_2O_3 content such as mullite $3(\text{Al}_2\text{O}_3)2(\text{SiO}_2)$ there seems to be a relatively large amount of five- and six-fold coordinated Al atoms in addition to AlO_4 units. And secondly, NMR experiments found evidence for the existence of a high amount of so-called triclusters, i.e. structural units where an oxygen atom is surrounded by three cations (whereby at least one of them is an aluminium atom) [19, 20, 21, 22, 23]. The possibility of such triclusters has been very recently confirmed in *ab initio*, molecular orbital calculations [27]. The presence of triclusters has been also discussed in the context of extensive viscosity measurements of $\text{Na}_2\text{O--Al}_2\text{O}_3\text{--SiO}_2$ liquids [28, 29].

As mentioned before, pure silica forms a network of corner-shared SiO_4 units and thus the O atoms are two-fold coordinated by Si atoms. The appearance of triclusters in amorphous aluminium silicates is an indication for the different local ordering of the different cationic species Al and Si. The difference in the local structure around the Al atoms from that around the Si atoms is accompanied by the tendency towards a metastable liquid–liquid phase separation below ≈ 1900 K for an Al_2O_3 content between about 10 to 50 mol% [4, 5, 6]. The system we consider in the following is approximately in the centre of the demixing region: By means of MD simulations we investigate an aluminium silicate melt with 33 mol% Al_2O_3 , i.e. $(\text{Al}_2\text{O}_3)_2(\text{SiO}_2)$, and in the following we will denote this system by AS2.

It is one of the merits of MD simulations that one can study at the same time the structure on local and medium length scales in conjunction with dynamic properties. The duration of the MD runs is of course restricted to time scales in the ns range and so we are not able to approach the experimentally expected liquid–liquid coexistence line very closely. However, as we demonstrate in the following, the simulations do shed light onto precursors of phase separation in the microscopic structure.

The rest of the paper is organized as follows: In the next section we give the details of the model and the simulation procedure. Then we present the results for the structure and diffusion in AS2, and finally we summarize and discuss them in the last section.

2 Model and details of the simulation

A potential that has often been used recently to study the properties of amorphous silica is the so-called BKS potential [30] that has been developed by van Beest, Kramer, and van Santen by means of *ab initio* calculations. Although it is a simple pair potential, it has been shown to reproduce very well many static and dynamic properties of amorphous silica [31, 32, 33, 34, 8, 35, 36, 37, 38, 39, 40, 41, 42, 43, 44]. An extension of the BKS potential that allows to consider also mixtures of silica with other oxides such as Na_2O and Al_2O_3 was proposed by Kramer *et al.* [45]. As demonstrated recently [46, 47, 14, 48, 15, 13, 49, 50], this potential gives also a quite realistic description of the static and dynamic properties of sodium silicates.

In this work we use the latter potential to investigate the aluminium silicate melt $(\text{Al}_2\text{O}_3)_2(\text{SiO}_2)$ [AS2]. The functional form of the potential is as follows:

$$\varphi_{\alpha\beta}(r) = \frac{q_\alpha q_\beta e^2}{r} + A_{\alpha\beta} \exp(-B_{\alpha\beta} r) - \frac{C_{\alpha\beta}}{r^6}, \quad (1)$$

where $\alpha, \beta \in \{\text{Si}, \text{Al}, \text{O}\}$. Here r is the distance between an ion of species α and an ion of species β . The values of the parameters $\{A_{\alpha\beta}, B_{\alpha\beta}, C_{\alpha\beta}\}$ that were calculated by *ab initio* methods are $A_{\text{SiO}} = 18003.7572$ eV, $A_{\text{AlO}} = 8566.5434$ eV, $A_{\text{OO}} = 1388.7730$ eV, $B_{\text{SiO}} = 4.87318 \text{ \AA}^{-1}$, $B_{\text{AlO}} = 4.66222 \text{ \AA}^{-1}$, $B_{\text{OO}} = 2.76 \text{ \AA}^{-1}$, $C_{\text{SiO}} = 133.5381 \text{ eV \AA}^6$, $C_{\text{AlO}} = 73.0913 \text{ eV \AA}^6$, and $C_{\text{OO}} =$

175.0 eVÅ⁶ (for the Si–Si, Si–Al and Al–Al interactions the latter parameters are all set to zero) [45].

From Eq. (1) it becomes obvious that at small distances the potential between the Al (or Si) and the O atoms goes to minus infinity (since the coefficients $C_{\alpha\beta}$ are positive), i.e. it becomes unphysical. Therefore we have modified the potential at short distances by substituting it with a simple parabola:

$$\varphi_{\text{AlO}} = -19.9508 \text{ eV} + 15.5 \frac{\text{eV}}{\text{\AA}^2} (r - 1.16576 \text{ \AA})^2 \quad r \leq 1.1658 \text{ \AA} . \quad (2)$$

We emphasize however, that this change hardly affects the properties of the system since at intermediate and low temperatures the probability of finding a distance below 1.17 Å between an Al and an O particle is very small. Note that we use similar modifications as the one given by Eq. (2) also for the Si–O and O–O interactions. Details can be found in Ref. [31].

In the long-ranged Coulomb-part the charges $q_\alpha e$ (e : charge of an electron) are not the bare ionic charges of ions of type α but are considered to be effective charges. Unfortunately in Ref. [45], the q_α 's were fixed such that systems like AS2 are not neutral: $q_{\text{O}} = -1.2$, $q_{\text{Si}} = 2.4$, and $q_{\text{Al}} = 1.9$. Only with the additional component phosphorus the system recovers charge neutrality according to the parameter sets in Ref. [45]. The same problem arises for sodium silicates if one uses the Kramer potential. In order to overcome this problem we follow here the same strategy that we have already applied in the case of the potential for the sodium silicates [46, 14, 48]: We set the charge of aluminium to $q_{\text{Al}}e = 1.8e$ such that a stoichiometric aluminium silicate system as AS2 is neutral. Then we add a short-ranged potential that compensates for this change at *short* distances. The final form of the potential is given by

$$\Phi_{\alpha\beta} = \varphi_{\alpha\beta} + \frac{\tilde{q}_\alpha \tilde{q}_\beta e^2}{r} [1 - (1 - \delta_{\alpha\text{Al}})(1 - \delta_{\beta\text{Al}})] \Theta(r_c - r) \quad , \quad (3)$$

with Θ being the Heaviside function, with $\tilde{q}_{\text{Si}} = 2.4$, $\tilde{q}_{\text{O}} = -1.2$, and

$$\tilde{q}_{\text{Al}}(r) = q_{\text{Al}} \left(1 + \ln \left[C \frac{(r_c - r)^2}{1 \text{\AA}^2 + (r_c - r)^2} + 1 \right] \exp \left(- \frac{d}{(r - r_c)^2} \right) \right) . \quad (4)$$

Here the parameters $r_c = 6.0 \text{ \AA}$, $C = 0.0653$, and $d = 2.0 \text{ \AA}^2$ are chosen. These parameters guarantee that the potential given by Eq. (3) is indeed very similar to the original one as illustrated in Fig. 1: For $r < 2.2 \text{ \AA}$ the modified potential is almost the same as the original one. Finally we mention that the presence of the exponential term in Eq. (4) makes that the charge q_{Al} is a smooth function of r .

The equations of motion were integrated with the velocity form of the Verlet algorithm using a time step of 1.6 fs. The Coulomb forces were calculated by the standard Ewald summation technique. At each temperature we equilibrated the system first in the NVT ensemble by coupling it to a stochastic heat bath. Thereby, the equilibration time exceeded the structural relaxation time

for the slowest component (i.e. silicon), i.e. dynamic density–density correlation functions for silicon at the wave–vector $q = 1.7 \text{ \AA}^{-1}$ (corresponding to the characteristic length scale of the tetrahedral network, see below) have decayed to zero in that time [51]. After equilibration the heat bath was switched off, and we started production runs in the microcanonical ensemble. During all runs the density was fixed to the experimental value at 300 K, $\rho = 2.60 \text{ g/cm}^3$ [52]. The number of particles was 1408 ($N_{\text{Si}} = 256$, $N_{\text{Al}} = 256$, $N_{\text{O}} = 898$) and hence the linear dimension of the cubic simulation box was $L = 26.347 \text{ \AA}$. The temperatures that we have investigated are 6100 K, 4700 K, 4000 K, 3580 K, 3250 K, 3000 K, 2750 K, 2600 K, 2480 K, 2380 K, and 2300 K. The production runs at the lowest temperature lasted over 6.9 ns real time corresponding to 4.2 million time steps. In addition we did cooling runs from 2300 K to 0 K with a constant cooling rate $\gamma = 1.42 \cdot 10^{12} \text{ K/s}$. At each temperature we did five completely independent runs in order to improve the statistics.

3 Results

In this section we present the results of our simulations. First, we study in detail the local structure of the network in AS2 and show then the consequences of the local chemical ordering for length scales that go beyond distances of nearest and next–nearest atoms. Finally, we discuss the behavior of the self–diffusion constants.

Before we start the discussion of structural quantities we present in Fig. 2 the pressure p as a function of temperature. From this graph we recognize that in the temperature range considered the pressure varies between 1 and 5 GPa. This strong variation is related to the fact that we have made our simulation at constant volume. It is, however, reassuring that at ambient temperature the pressure is not exceedingly high, thus showing that the potential is quite reliable with respect to the pressure. Furthermore we point out that it is unlikely that for a system like AS2 the structure changes significantly in the pressure range that we have here. Therefore we expect that the results presented here are very similar to the ones that one would get in a constant pressure simulation.

It is remarkable that $p(T)$ exhibits a local minimum around $T = 2500 \text{ K}$ which would correspond to a density maximum in a constant pressure simulation. So our model predicts for AS2 a density anomaly which is a well–known feature in amorphous silica [53]. Note that for $T < 2300 \text{ K}$ the system is no longer in equilibrium but in the glass phase. From the fact that in this temperature range $p(T)$ shows basically a linear variation with temperature, we thus can conclude that anharmonic effects are not important.

Quantities that are well suited to characterize the local structure of atomic systems are the partial pair correlation functions $g_{\alpha\beta}(r)$ which are proportional to the probability of finding a particle of type β at a distance r from a particle of type α . The definition of $g_{\alpha\beta}(r)$ can be found in standard textbooks [54]. The six different $g_{\alpha\beta}(r)$ of our system are shown in Fig. 3 for the three temperatures $T = 4000 \text{ K}$, 2300 K , and 300 K . The sharp first peak around $r = 1.605 \text{ \AA}$ in

$g_{\text{SiO}}(r)$ reflects the strong covalent nature of the Si–O bond. We also can note that in the first minimum of $g_{\text{SiO}}(r)$, which is around 2.3 Å, the function is basically zero even at 4000 K. Thus this feature allows for a natural definition of nearest neighbors of a silicon atom, and below we will make use of this fact. Moreover, there is a gap between 2 Å and 3 Å which is due to the chemical ordering in the network of AS2: In between a silicon atom and a second nearest oxygen neighbor there must be always another silicon (or aluminium) atom. The functions $g_{\text{AlO}}(r)$ look very similar to $g_{\text{SiO}}(r)$ at the corresponding temperature, but the former are less pronounced in that the first peak is slightly broader and it has a smaller amplitude. Furthermore, the position of the first peak in $g_{\text{AlO}}(r)$ is now at the slightly higher value $r = 1.66$ Å. This is in agreement with experiments and *ab initio* simulations of similar systems, although slightly higher values between 1.71 Å and 1.77 Å have been reported [55, 56].

Significant differences are found between $g_{\text{AlAl}}(r)$ and $g_{\text{SiSi}}(r)$: At 300 K the first peak in $g_{\text{AlAl}}(r)$ splits up in two peaks at $r_1 = 2.59$ Å and $r_2 = 3.16$ Å whereas in $g_{\text{SiSi}}(r)$ one finds only a single peak at about 3.12 Å, i.e. a value very similar to r_2 . Also in $g_{\text{SiAl}}(r)$ one finds a shoulder around r_1 . We will see below that the feature around r_1 is due to the presence of two-membered rings. Fig. 3c shows a comparison of $g_{\text{OO}}(r)$ for AS2 with that for SiO_2 at $T = 300$ K (the latter was taken from a recent simulation study, for details see Ref. [8]). The main difference is that the first peak in the function for AS2 is shifted to larger distances which stems from the fact that the length of an Al–O bond is slightly larger than the length of a Si–O bond.

In pure SiO_2 a disordered tetrahedral network is formed such that a silicon atom sits in the centre of each tetrahedron, whereby the oxygen atoms at the four corners of this tetrahedron are shared by the silicon atoms of the two neighboring tetrahedra (and thus each oxygen atom is two-fold coordinated by silicon atoms). It was shown in a MD simulation of a SiO_2 model [8]) that this local structure is essentially formed at temperatures as high as 3000 K since even at this temperature the percentage of defects (such as a Si atom that is five-fold coordinated by O atoms or an O atom that is three-fold coordinated by Si atoms) is smaller than 5 %.

We demonstrate now that the structure of our AS2 model is far from a perfect tetrahedral network even at very low temperatures. To this end, we consider coordination number distributions $P_{\alpha\beta}(z)$ which give the probability that a particle of type α is surrounded by exactly z neighbors of type β within a distance $r \leq r_{\min}^{\alpha\beta}$ (where $r_{\min}^{\alpha\beta}$ corresponds to the first minimum in $g_{\alpha\beta}(r)$). Fig. 4 shows $P_{\alpha\beta}(z)$ for Si–O, Al–O, O–(Si,Al), O–Si, and O–Al correlations (O–(Si,Al) means that one does not distinguish between Si and Al atoms) at the three temperatures 4000 K, 2750 K, and 300 K. The values used for $r_{\min}^{\alpha\beta}$ are $r_{\min}^{\text{SiO}} = 2.33$ Å, $r_{\min}^{\text{AlO}} = 2.54$ Å for $T = 4000$ K, $r_{\min}^{\text{SiO}} = 2.25$ Å, $r_{\min}^{\text{AlO}} = 2.42$ Å for $T = 2750$ K, and $r_{\min}^{\text{SiO}} = 2.20$ Å, $r_{\min}^{\text{AlO}} = 2.40$ Å for $T = 300$ K. As we can infer from P_{SiO} and P_{AlO} , at low temperatures most of the Si and Al atoms are four-fold coordinated by O atoms and thus also Al is integrated in the tetrahedral network structure. Note that also a recent MD simulation of a realistic model

of a pure Al_2O_3 melt finds a structure at low temperatures in which most of the Al atoms are four-fold coordinated by O atoms [57].

That the packing of the AlO_4 tetrahedra is nevertheless different from that of the SiO_4 tetrahedra is demonstrated in Figs. 4c and 4d. Only 70% of the O atoms are two-fold coordinated but around 30% of the O atoms are three-fold coordinated by (Si,Al) atoms, thus forming the so-called triclusters that have been identified in NMR experiments. It is remarkable that the percentage of such triclusters is nearly independent of temperature in our simulations. The distributions P_{OSi} and P_{OAl} show that the probability that an O atom is three-fold coordinated by silicon atoms is very low (essentially zero at 300 K), whereas the probability for triclusters with three Al atoms is relatively high and increases even slightly with decreasing temperature. A closer inspection at $T = 300$ K shows the following cation composition of the triclusters: There are 1.4% with three Si, 12.4% with two Si and one Al, 47.3% with one Si and two Al, and 38.9% with three Al. So most triclusters contain one Si and two Al atoms or three Al atoms.

We have seen that at low temperatures most of the Al atoms are four-fold coordinated by oxygens. On the other hand there are two different characteristic length scales r_1 and r_2 for the distance between nearest Al neighbors. These two length scales should be also reflected in the geometry of the AlO_4 tetrahedra: Two connected tetrahedra for which the Al atoms are at a distance r_1 from each other may have a different geometry from two connected tetrahedra where the two aluminium atoms in the centres are at distance around r_2 . Appropriate quantities to study the geometry of the tetrahedra are $P_{\alpha\beta\gamma}(\theta)$, the distribution for the O–Si–O and O–Al–O angles, which are shown in Fig. 5. In $P_{\text{OSiO}}(\theta)$ a single peak is observed which, by decreasing the temperature, becomes sharper and the location of the maximum moves to larger angles. At $T = 300$ K the maximum is at $\theta = 108.2^\circ$ which is close to the value for an ideal tetrahedron, $\theta = 109.47^\circ$ (vertical lines). The behavior of $P_{\text{OAlO}}(\theta)$ is very different in that one finds at $T = 300$ K two peaks: $\theta_1 = 85.8^\circ$ and $\theta_2 = 109.8^\circ$. Such a bimodal distribution has been found also in computer simulations of free silica surfaces [38, 39] where one obtains two peaks in $P_{\text{OSiO}}(\theta)$ for the surface region at similar values for θ_1 and θ_2 . And also in this case the bimodal distribution of angles is accompanied by two “nearest neighbor peaks” in $g_{\text{SiSi}}(r)$. The authors of Refs. [38, 39] have explained these features at free silica surfaces by the presence of two-membered rings, i.e. structural units where two tetrahedra share two oxygen atoms. The two tetrahedra that form the two-membered rings are deformed such that the distance between the two cations is at r_1 and the O–cation–O angles are at θ_1 . (Here the two oxygens are of course the shared O atoms.) There is one major difference between the two-membered rings of free silica surfaces and the ones in AS2: In the former case they become very rare at low temperatures whereas in the case of AS2 their occurrence increases slightly with temperature.

Apart from two-membered rings it is also straightforward to define rings of any size n in the network: One selects any cation (i.e. Si or Al) and two of its O neighbors. There are several possible paths how one can move through

the network structure from one cation–O pair to the next one such that one starts from the pair with the first O atom and ends at a cation–O pair with the second O atom. The shortest possible of such paths are called rings and the length of a ring is the number of cation–O pair that it contains. In Fig. 6 the ring size distribution $P(n)$ is shown for three different temperatures. Whereas $P(n)$ changes significantly from 4000 K to 2300 K, only minor changes are observed from 2300 K to 300 K. However, we recognize essentially the same qualitative behavior at the three temperatures: most probable are rings with a size of $n = 5$ and there is a relatively large contribution of rings with $n = 2$ and $n = 3$. Note that the location of the maximum at $n = 5$ is different from that which one expects for pure silica at low temperatures where MD simulations have found the maximum at $n = 6$ (corresponding to the length of the rings in β -cristobalite) [31, 58].

We have also determined the composition of small-membered rings at $T = 300$ K yielding for the rings with $n = 2$ that 72.8% consist of two Al atoms, 25.0% contain one Al and one Si atom, and there are 2.2% with two Si atoms. For the three-membered rings we obtain the following numbers: 36.5% with three Al atoms, 45.3% with two Al and one Si atom, 15.5% with one Al and two Si atoms, and 2.7% with three Si atoms.

One may ask whether the relatively high probability of two-membered rings in our AS model is related to the occurrence of the aforementioned triclusters. And indeed we have extracted from our data that at $T = 300$ K 96% percent of the oxygen atoms that are involved in a tricluster are also a member of a ring with $n = 2$. And this holds also the other way round: more than 95% of the O atoms that are members in any two-membered ring are three-fold coordinated by cations and form thus a tricluster. So we find that the appearance of triclusters in our AS2 model is accompanied by the presence of two-membered rings which to our knowledge is a connection that has not been considered yet in the analysis of experiments. A typical local configuration with a two-membered Al–O ring and two triclusters is illustrated by a schematic picture in Fig. 7.

The results discussed so far have shown that the aluminium atoms do form tetrahedral units with oxygens but that the packing of these AlO_4 units is very different from the one of the SiO_4 units. We now want to study whether the different local order around Al and Si atoms leads to structural features that are present on larger length scales. To this end, we consider partial static structure factors which are the Fourier transforms of the corresponding pair correlation functions. They are correlation functions of the number densities

$$\rho_\alpha(\mathbf{q}) = \sum_{k=1}^{N_\alpha} \exp(i\mathbf{q} \cdot \mathbf{r}_k) \quad \alpha \in \{\text{Si, Al, O}\} \quad (5)$$

(depending on wave-vector \mathbf{q}) and can be defined as follows [54]:

$$\begin{aligned} S_{\alpha\beta}(q) &= \frac{1}{N} \langle \rho_{\alpha}(\mathbf{q}) \rho_{\beta}(-\mathbf{q}) \rangle \\ &= \frac{f_{\alpha\beta}}{N} \sum_{k=1}^{N_{\alpha}} \sum_{l=1}^{N_{\beta}} \langle \exp(i\mathbf{q} \cdot (\mathbf{r}_k - \mathbf{r}_l)) \rangle, \end{aligned} \quad (6)$$

with N being the total number of particles, q is the absolute value of the wave-vector \mathbf{q} , and $f_{\alpha\beta}$ is equal to 0.5 if $\alpha \neq \beta$ and to 1.0 if $\alpha = \beta$. Fig. 8 shows $S_{\alpha\beta}(q)$ at the three temperatures $T = 4000$ K, 2300 K, and 300 K. Similar to the results found for the radial distribution functions, the temperature dependence of $S_{\alpha\beta}(q)$ is relatively weak in that the different peaks that are found at low temperatures are already present at a temperature as high as 4000 K. For $q > 2.3 \text{ \AA}^{-1}$ the partial structure factors reflect length scales of nearest neighbors and their location corresponds approximately to the period of oscillations in the $g_{\alpha\beta}(r)$. But we are now more interested in the features in $S_{\alpha\beta}(q)$ at small q . The peaks at $1.6\text{--}1.7 \text{ \AA}^{-1}$ are due to the order that arises from the tetrahedral network structure, i.e. from repeated AlO_4 and SiO_4 units. And indeed the length $2\pi/(1.7 \text{ \AA}^{-1}) = 3.7 \text{ \AA}$ corresponds approximately to the spatial extent of two connected tetrahedra. Note that a prepeak around $q = 1.7 \text{ \AA}^{-1}$ in the static structure factor is also found in pure silica and in many other materials that form tetrahedral networks (e.g. see Ref. [31] and references therein).

But from Fig. 8 we recognize that there is also an additional prepeak at $q = 0.5 \text{ \AA}^{-1}$ in the $S_{\alpha\beta}(q)$ for the Si-Si, Al-Al, and Si-Al correlations. One possible explanation for this peak is the following one: As we have seen in our analysis of the local structure before, the local packing of AlO_4 tetrahedra is significantly different from that of the SiO_4 tetrahedra. This may lead to a structure where an AlO_4 tetrahedron prefers to be surrounded by other AlO_4 tetrahedra and thus Al rich regions are formed. So a structure is created where the Al atoms are not homogeneously distributed on the relatively large length scale $l \approx 2\pi/(0.5 \text{ \AA}^{-1}) \approx 12.6 \text{ \AA}$. If one considers only the Al atoms for instance, voids are formed with the spatial extent given by l in the regions where the Si atoms sit. The same holds of course true if one considers only the Si atoms. In the $S_{\alpha\beta}(q)$ in which the O atoms are involved, almost no peak at 0.5 \AA^{-1} is seen because the oxygen atoms are essentially homogeneously distributed in the system on the length scale l since they are both nearest neighbors of Si and Al atoms (the difference in the chemical ordering of the O atoms around the Al atoms from that around the Si atoms is only weakly pronounced on the length scale l).

The structure of our AS2 model at $T = 300$ K is illustrated by a snapshot of the simulation box, Fig. 9. (Note that the size of the shown atoms does not correspond to their actual size.) One can clearly see that Al rich regions are formed that percolate through the SiO_4 network. From this figure it is also visible that the packing of the AlO_4 tetrahedra is denser due to the formation of more compact structural units such as small-membered rings.

If our interpretation of the prepeak at 0.5 \AA^{-1} is correct then it should be present in a pronounced way in static concentration fluctuations. For a mixture with the two components A and B the static concentration–concentration structure factor $S_{cc}(q)$ can be easily computed from the partial structure factors $S_{\alpha\beta}(q)$ [54]:

$$S_{cc}(q) = x_B^2 S_{AA}(q) + x_A^2 S_{BB}(q) - 2x_A x_B S_{AB}(q) \quad (7)$$

with $x_A = N_A/N$ and $x_B = N_B/N$ being the concentration of A and B particles, respectively. For our three–component system we may also use Eq. (7) in the following way: We do not distinguish between two of the three species such that for instance the A species combines Si and O particles and the B species is given by the Al particles. For this example the functions $S_{AA}(q)$, $S_{AB}(q)$, and $S_{BB}(q)$ are then given by

$$\begin{aligned} S_{AA}(q) &= S_{\text{SiSi}} + S_{\text{OO}} + 2S_{\text{SiO}} , \\ S_{AB}(q) &= S_{\text{SiAl}} + S_{\text{AlO}} , \\ S_{BB}(q) &= S_{\text{AlAl}} , \end{aligned}$$

and from these functions a structure factor $S_{cc}(q)$ can be calculated by Eq. (7) whereby $N_A = N_{\text{Si}} + N_{\text{O}}$ and $N_B = N_{\text{Al}}$. The latter concentration–concentration structure factor is nothing else than the static autocorrelation function of the concentration density c_{Al} of the Al atoms [59,60]. In an analogous way one can calculate two other structure factors for AS2 that correspond to the autocorrelation functions of the concentration densities for Si and O, respectively. Thus, in terms of the concentration densities

$$c_\alpha(\mathbf{q}) = \rho_\alpha(\mathbf{q}) - x_\alpha (\rho_{\text{Si}}(\mathbf{q}) + \rho_{\text{Al}}(\mathbf{q}) + \rho_{\text{O}}(\mathbf{q})) \quad \alpha \in \{\text{Si}, \text{Al}, \text{O}\} \quad (8)$$

with $x_\alpha = N_\alpha/N$, the latter three concentration–concentration structure factors are defined by

$$S_{c_\alpha c_\alpha}(q) = \frac{1}{N} \langle c_\alpha(\mathbf{q}) c_\alpha(-\mathbf{q}) \rangle . \quad (9)$$

More details on the $S_{c_\alpha c_\alpha}(q)$ can be found in Refs. [59,60].

The three functions $S_{c_\alpha c_\alpha}(q)$ are shown in Fig. 10 for $T = 300 \text{ K}$. In all three functions a pronounced peak is seen around $q = 2.72 \text{ \AA}^{-1}$ corresponding to the length scale of nearest Si–Si, Al–Al etc. neighbors. This is reasonable since there should be strong concentration fluctuations on this length scale due to the chemical ordering in the tetrahedral network of AS2. Furthermore we do also find a well–pronounced peak around 0.5 \AA^{-1} in $S_{c_{\text{Al}} c_{\text{Al}}}(q)$ and $S_{c_{\text{Si}} c_{\text{Si}}}(q)$ which confirms our interpretation of this prepeak. Also in accordance with our interpretation is that no prepeak around 0.5 \AA^{-1} is seen in $S_{c_{\text{O}} c_{\text{O}}}(q)$ because the O atoms are ordered in a similar way around the cations and so in $S_{c_{\text{O}} c_{\text{O}}}(q)$ no distinction is made between Si rich and Al rich regions.

Of course the question arises whether it is possible to observe the prepeak at 0.5 \AA^{-1} also in experiments, i.e. whether or not real AS2 shows a structure on the length scale of 12.6 \AA . Unfortunately in experiments such as neutron

scattering one does not have access to the partial structure factors for systems like AS2 (due to the lack of appropriate isotopes) and one can only measure a linear combination of the partial structure factors (in the case of neutron scattering the $S_{\alpha\beta}(q)$ are weighted by the neutron scattering lengths). As it is shown elsewhere [51], in such a quantity one can hardly identify the prepeak at 0.5 \AA^{-1} because at small wave-vectors the dominant contribution comes from $S_{\text{OO}}(q)$, a partial structure factor which does not show the prepeak. So it remains a challenge to the experimentalists to develop techniques with which one can verify the presence of the latter prepeak in AS2.

However, in order to see how far our microscopic model is able to reproduce the structure of real AS2, we compare now the “reduced” total static X-ray scattering factor of AS2, $q(S_X(q) - 1)$, as obtained from our simulation to an experimental result. $S_X(q)$ can be calculated from the $S_{\alpha\beta}(q)$ by weighting them with X-ray form factors:

$$S_X(q) = \frac{N}{\sum_{\alpha} N_{\alpha} f_{\alpha}^2(s)} \sum_{\alpha\beta} f_{\alpha}(s) f_{\beta}(s) S_{\alpha\beta}(q) , \quad (10)$$

with $\alpha, \beta \in \{\text{Si}, \text{Al}, \text{O}\}$. The formfactors $f_{\alpha}(s)$ depend on the wave-vector q via $s = q/4\pi$. We have taken the $f_{\alpha}(s)$ from Ref. [61]. Fig. 11 shows $S_X(q)$ as calculated from our simulation by Eq. (10) in comparison to the experimental result of Morikawa *et al.* [24] for an aluminium silicate melt with 37.1 mol% Al_2O_3 , i.e. a composition which is slightly different from that of AS2 (AS2 contains 33.3 mol% Al_2O_3). As we recognize from Fig. 11 the agreement between simulation and experiment is particularly good for $q < 2.3 \text{ \AA}^{-1}$ and also a fair agreement is obtained for higher q .

Finally, we want to turn our attention to the diffusion dynamics of the AS2 melt. The self-diffusion constant D_{α} for a particle of type $\alpha \in \{\text{Si}, \text{Al}, \text{O}\}$ can be calculated from the mean squared displacements $\langle r_{\alpha}^2(t) \rangle$ via the Einstein relation:

$$D_{\alpha} = \lim_{t \rightarrow \infty} \frac{\langle r_{\alpha}^2(t) \rangle}{6t} . \quad (11)$$

In Fig. 12 the three different D_{α} for AS2 are plotted on a semi-logarithmic scale as a function of inverse temperature. Also included are D_{Si} and D_{O} of pure silica from a recent MD simulation [8]. At $T = 6100 \text{ K}$ the $D_{\alpha}(T)$ in AS2 are very similar to those in SiO_2 . However, upon decreasing the temperature, the dynamics in AS2 does not slow down as rapidly as the one of SiO_2 . At $T = 2750 \text{ K}$ the diffusion of all components in AS2 is about two orders of magnitude faster than in SiO_2 . The self-diffusion constants in SiO_2 show a crossover from a power law behavior as predicted by the mode coupling theory (MCT) of the glass transition [62] at high temperatures (see dashed lines in Fig. 12) to an Arrhenius behavior at low temperatures whereby we have found the critical mode coupling temperature at 3330 K (for more details see Refs. [8, 35]). A similar analysis as the one in SiO_2 for AS2 is the subject of future work. As we see in Fig. 12 the self-diffusion in AS2 provides the very interesting case of a tetrahedral network where the dynamics of one of the cations, aluminium,

is slightly faster than that of oxygen whereas the diffusion of the other cation, silicon, is a factor of 2 or 3 slower than that of oxygen.

In order to quantify further the difference in the temperature dependence of the different diffusion constants, we show in Fig. 13 the ratios $D_{\text{Si}}/D_{\text{O}}$, $D_{\text{Si}}/D_{\text{Al}}$, $D_{\text{Al}}/D_{\text{O}}$ for AS2 as well as $D_{\text{Si}}/D_{\text{O}}$ for SiO_2 as a function of temperature. $D_{\text{Si}}/D_{\text{O}}$ for SiO_2 varies only from 0.65 to 0.8 in the temperature range $3400 \text{ K} \leq T \leq 6100 \text{ K}$, whereas it decreases rapidly below about 3400 K. The latter behavior can be explained by a change in the transport mechanism around the critical MCT temperature $T_c = 3330 \text{ K}$ of our SiO_2 model (for more details see Refs. [8, 35]). As mentioned before, in the case of AS2 it is an open question whether one can understand the diffusion dynamics by means of MCT. However, $D_{\text{Si}}/D_{\text{O}}$ and $D_{\text{Si}}/D_{\text{Al}}$ exhibit a very similar behavior as $D_{\text{Si}}/D_{\text{O}}$ in SiO_2 . It is remarkable that $D_{\text{Al}}/D_{\text{O}}$ seems to approach a constant value for temperatures below about 3000 K, an issue that has to be clarified also in future studies.

4 Summary and conclusions

In this paper we have presented the results of large scale molecular dynamics computer simulations to investigate the structure and diffusion dynamics of the amorphous aluminium silicate melt $(\text{Al}_2\text{O}_3)_2(\text{SiO}_2)$ [AS2]. The microscopic interactions were described by a simple pair potential that has been determined by Kramer *et al.* [45] using *ab initio* calculations.

It is one of the open questions in the literature on aluminium silicate melts and glasses how the local structure around an aluminium atom evolves in order to yield charge neutrality on a local scale. We find in the simulations of our AS2 model that, similar to the Si atoms, already at high temperatures most of the Al atoms are four-fold coordinated by O atoms. However, the packing of the AlO_4 tetrahedra is denser than that of the SiO_4 tetrahedra which is manifested especially in the presence of 3(Al,Si) triclusters. Evidence for such structural units in systems like AS2 has been given in NMR experiments [19, 20, 21, 22, 23]. Our simulation allows a detailed description of the geometry of the triclusters: We find that in most of them the three-fold coordinated O atoms are members of a two-membered ring (whereby these rings contain most likely two aluminium atoms). Furthermore, we find also a relatively high occurrence of three-membered rings in AS2 in which most likely at least two Al atoms participate. In contrast to the small-membered rings in SiO_2 , Al rings in AS2 of length two or three become slightly more frequent if one cools down the system to low temperatures.

Similar structural features as in our AS2 model have been found recently also in a MD simulation of pure amorphous aluminium oxide (Al_2O_3) [57]. Also in that case a high number of small-membered rings was found, in particular also a relatively high number of two-membered rings. The geometry of the latter rings is slightly different from that in AS2 since in Al_2O_3 (at least as far as it is predicted in the simulation) it is not the presence of two edge-sharing AlO_4 tetrahedra that is very likely but either two edge-sharing AlO_5 polyhedra or an

AlO_4 tetrahedron sharing an edge with an AlO_5 unit. However, the presence of two-membered rings in a model of Al_2O_3 and in a model of AS2 (based on completely different *ab initio* calculations) may indicate that two-membered Al rings are indeed a typical structural unit in melts and glasses containing Al_2O_3 and thus, this finding is worth to be checked in experiments.

The difference in the local environment of the Al and the Si atoms leads to the formation of Al rich regions such that a network of AlO_4 units percolates through the SiO_4 structure. The characteristic length scale of the latter structure is reflected by a prepeak in the static structure factor at $q \approx 0.5 \text{ \AA}^{-1}$. This prepeak can be seen as the manifestation of a microphase separation and indeed, in accordance with this interpretation, it is a pronounced feature in static structure factors of concentration densities as defined by Eq. (7) (see Fig. 10). The presence of a microphase separation in the melt structure is another prediction of our simulation that could be checked in experiments. Of course, as we have shown above, this is not a simple task.

It is interesting that prepeaks with a physical origin as the one in our AS2 model have been found also for other binary silicate melts, e.g. in sodium silicates at $q = 0.95 \text{ \AA}^{-1}$ both in simulation and neutron scattering or in a calcium silicate glass at $q = 1.3 \text{ \AA}^{-1}$ by means of neutron scattering [63].

The critical point of the demixing transition in the experimental phase diagram of Al_2O_3 - SiO_2 is at $\approx 1920 \text{ K}$ for a mixture with $\approx 30 \text{ mol\% Al}_2\text{O}_3$ [6]. Thus, if the model used in this work exhibits a similar phase diagram as real systems, AS2 is close to the critical composition and the lowest temperature used in this work above the glass transition, $T = 2300 \text{ K}$, is only a few hundred Kelvin above the critical temperature. In this sense, the observed microphase separation can be seen as the precursor of a critical unmixing transition. In this context it is interesting to study how the dynamics is affected by a possible interplay between structural relaxation and a critical slowing down. It has recently been shown that mode coupling theory (MCT) describes the slowing down due to structural relaxation in systems like SiO_2 or $(\text{Na}_2\text{O})_2(\text{SiO}_2)$ very well [8, 35, 48] (this holds above and around the critical temperature of MCT). In AS2 the case might occur where the scenario for structural relaxation as predicted by MCT interferes with the critical dynamics near a second order demixing transition.

In order to shed light on these guesses it is necessary to determine the phase diagram of the model and this requires the use of techniques that are different from Molecular Dynamics: Well-suited in this case are Monte-Carlo simulations in the semi-grandcanonical ensemble in conjunction with multicanonical sampling [64]. These methods have also the advantage that they yield configurations exactly on the coexistence line of the demixing transition which can be used as starting configurations for Molecular Dynamics simulations to study the microscopic structure and dynamics. The latter procedure has recently been successfully used for a symmetrical Lennard-Jones mixture [65]. Therefore it can be hoped that the application of this technique will also be useful for more complex systems like AS2 and thus will help to increase our understanding of this glass-former.

Acknowledgments: This work was supported by SCHOTT Glas. Generous grants of computing time on CRAY-T3E at the NIC Jülich and the HLRS Stuttgart are gratefully acknowledged.

References

- [1] See, e.g., J. F. Stebbins, P. F. McMillan, and D. B. Dingwell (Eds.), Rev. in Mineralogy **32** (1995).
- [2] See, e.g., H. Bach and D. Krause (Eds.), *Analysis of the Composition and Structure of Glass and Glass Ceramics* (Springer, Berlin, 1999).
- [3] An overview on the recent research on ion-conducting mixtures can be found in K. L. Ngai, *Proc. of the 4th International Discussion meeting in Complex Systems*, J. Non-Cryst. Solids **307–310** (2002).
- [4] J. Hlaváč, *The Technology of Glass and Ceramics – An Introduction* (Elsevier, Amsterdam, 1983).
- [5] H. Rawson, *Properties and Applications of Glass* (Elsevier, Amsterdam, 1980).
- [6] J. F. MacDowell and G. H. Beall, J. Am. Ceramic Soc. **52**, 17 (1969).
- [7] A review of the simulation of silicate melts can be found in P. H. Poole, P. F. McMillan, and G. H. Wolf, Rev. in Mineralogy **32**, 563 (1995).
- [8] J. Horbach and W. Kob, Phys. Rev. B **60**, 3169 (1999).
- [9] C. Oligschleger, Phys. Rev. B **60**, 3182 (1999).
- [10] M. D. Ingram, Phys. Chem. Glasses **28**, 215 (1987); Phil. Mag. B **60**, 729 (1989).
- [11] W. Smith, G. N. Greaves, and M. J. Gillan, J. Chem. Phys. **103**, 3091 (1995).
- [12] J. Oviedo and J. F. Sanz, Phys. Rev. B **58**, 9047 (1998).
- [13] P. Jund, W. Kob, and R. Jullien, Phys. Rev. B **64**, 134303 (2001).
- [14] J. Horbach, W. Kob, and K. Binder, Phys. Rev. Lett. **88**, 125502 (2002).
- [15] J. Horbach, W. Kob, and K. Binder, J. Phys.: Condens. Matter **15**, S903 (2003).
- [16] A. Meyer, H. Schober, and D. B. Dingwell, Europhys. Lett. **59**, 708 (2002).
- [17] S. H. Risbud, R. J. Kirkpatrick, A. P. Taglialavore, and B. Montez, J. Am. Ceram. Soc. **70**, C10 (1987).

- [18] R. K. Sato, P. F. McMillan, P. Dennison, and R. Dupree, *J. Phys. Chem.* **95**, 4483 (1991).
- [19] B. T. Poe, P. F. McMillan, B. Coté, D. Massiot, and J.-P. Coutures, *J. Phys. Chem.* **96**, 8220 (1992); B. T. Poe, P. F. McMillan, C. A. Angell, and R. K. Sato, *Chem. Geol.* **96**, 333 (1992).
- [20] R. H. Meinhold, R. C. T. Slade, and T. W. Dawies, *Appl. Magn. Reson.* **4**, 141 (1993).
- [21] M. Schmücker and H. Schneider, *Ber. Bunsenges. Phys. Chem.* **100**, 1550 (1996).
- [22] M. Schmücker, K. J. D. MacKenzie, H. Schneider, and R. Meinhold, *J. Non-Cryst. Solids* **217**, 99 (1997).
- [23] M. Schmücker, H. Schneider, K. J. D. MacKenzie, and M. Okuno, *J. Eur. Ceramic Soc.* **19**, 99 (1999).
- [24] H. Morikawa, S.-I. Miwa, M. Miyake, F. Marum, and T. Sata, *J. Am. Ceramic Soc.* **65**, 78 (1982).
- [25] P. F. McMillan and B. Piriou, *J. Non-Cryst. Solids* **53**, 279 (1982).
- [26] M. Okuno, N. Zotov, M. Schmücker, and H. Schneider, submitted to *J. Non-Cryst. Solids* (2003).
- [27] J. D. Kubicki and M. J. Toplis, *Am. Mineral.* **87**, 668 (2002).
- [28] M. J. Toplis, D. B. Dingwell, K. U. Hess, and T. Lenci, *Am. Mineral.* **82**, 979 (1997).
- [29] M. J. Toplis, D. B. Dingwell, and T. Lenci, *Geochim. Cosmochim. Acta* **61**, 2605 (1997).
- [30] B. W. H. van Beest, G. J. Kramer, and R. A. van Santen, *Phys. Rev. Lett.* **64**, 1955 (1990).
- [31] K. Vollmayr, W. Kob, and K. Binder, *Phys. Rev. B* **54**, 15808 (1996).
- [32] J.-L. Barrat, J. Badro, and P. Gillet, *Mol. Sim.* **20**, 17 (1997).
- [33] M. Hemmati and C. A. Angell, in *Physics meets Geology*, H. Aoki and R. Hemley, Eds. (Cambridge University Press, Cambridge, 1998).
- [34] J. Horbach, W. Kob, and K. Binder, *J. Phys. Chem. B* **103**, 4104 (1999).
- [35] J. Horbach and W. Kob, *Phys. Rev. E* **64**, 041503 (2001).
- [36] J. Horbach, W. Kob, and K. Binder, *Eur. Phys. J. B* **19**, 531 (2001).
- [37] P. Scheidler, W. Kob, A. Latz, J. Horbach, and K. Binder, *Phys. Rev. B* **63**, 104204 (2001).

- [38] A. Roder, W. Kob, and K. Binder, J. Chem. Phys. **114**, 7602 (2001).
- [39] C. Mischler, W. Kob, and K. Binder, Comp. Phys. Comm. **147**, 222 (2002);
C. Mischler, Ph.D. Thesis, Universität Mainz, 2002.
- [40] P. Jund and R. Jullien, Phys. Rev. B **59**, 13707 (1999).
- [41] M. Benoit, S. Ispas, P. Jund, and R. Jullien, Eur. Phys. J. B **13**, 631 (2000).
- [42] D. J. Lacks, Phys. Rev. Lett. **84**, 4629 (2000).
- [43] I. Saika-Voivod, F. Sciortino, and P. H. Poole, Phys. Rev. E **63**, 011202 (2001).
- [44] M. S. Shell, P. G. Debenedetti, and A. Z. Panagiotopoulos, Phys. Rev. E **66**, 011202 (2002).
- [45] G. J. Kramer, A. J. M. de Man, and R. A. van Santen, J. Am. Chem. Soc. **113**, 6435 (1991).
- [46] J. Horbach and W. Kob, Phil. Mag. B **79**, 1981 (1999).
- [47] J. Horbach, W. Kob, and K. Binder, Chem. Geol. **174**, 174 (2001).
- [48] J. Horbach and W. Kob, J. Phys.: Condens. Matter **14**, 9237 (2002).
- [49] S. Ispas, M. Benoit, P. Jund, and R. Jullien, Phys. Rev. B **64**, 214206 (2001).
- [50] A. Winkler, J. Horbach, W. Kob, and K. Binder, to be published.
- [51] A. Winkler, Ph.D. Thesis, Universität Mainz, 2002.
- [52] O. V. Mazurin, M. V. Streltsina, and T. P. Shvaiko-Shvaikovskaya, *Handbook of Glass Data, Part A: Silica Glass and Binary Silicate Glasses* (Elsevier, Amsterdam, 1983).
- [53] R. Brückner, J. Non-Cryst. Solids **5**, 123 (1970).
- [54] J.-P. Hansen and I. R. McDonald, *Theory of Simple Liquids* (Academic, London, 1986).
- [55] M. Benoit, S. Ispas, and M. E. Tuckerman, Phys. Rev. B **64**, 224205 (2001).
- [56] R. D. Shannon, Acta Crystallogr. Sect. A **32**, 751 (1976).
- [57] G. Gutiérrez and B. Johansson, Phys. Rev. B **65**, 104202 (2002).
- [58] J. P. Rino, I. Ebbsjö, R. K. Kalia, A. Nakano, and P. Vashishta, Phys. Rev. B **47**, 3053 (1993).
- [59] J. Blétry, Z. Naturforsch. **31a**, 960 (1976).

- [60] J. Horbach, submitted to J. Non-Cryst. Solids (2003).
- [61] International Union of Crystallography (Ed.), *International Tables for X-ray Crystallography* (Kynoch Press, 1974), vol. 4, chap. 2.2, pp. 71–99.
- [62] W. Götze and L. Sjögren, Rep. Prog. Phys. **55**, 241 (1992); W. Götze, J. Phys.: Condens. Matter **10**, A1 (1999).
- [63] P. H. Gaskell, M. C. Eckersley, A. C. Barnes, and P. Chieux, Nature **350**, 675 (1991).
- [64] D. P. Landau and K. Binder, *A Guide to Monte Carlo Simulations in Statistical Physics* (Cambridge University Press, Cambridge, 2000).
- [65] S. K. Das, J. Horbach, and K. Binder, J. Chem. Phys. **119** (2003).

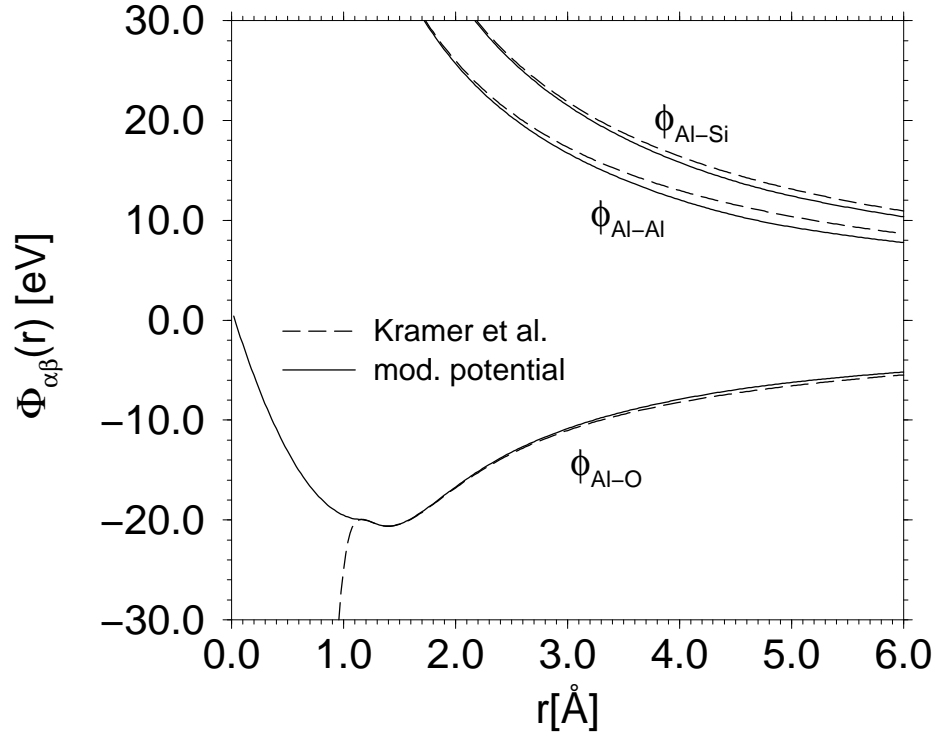


Figure 1: Al-Si, Al-Al and Al-O interaction potentials as proposed by Kramer *et al.* [45] (dashed lines) and in the modified version (solid lines) according to Eqs. (3)–(2).

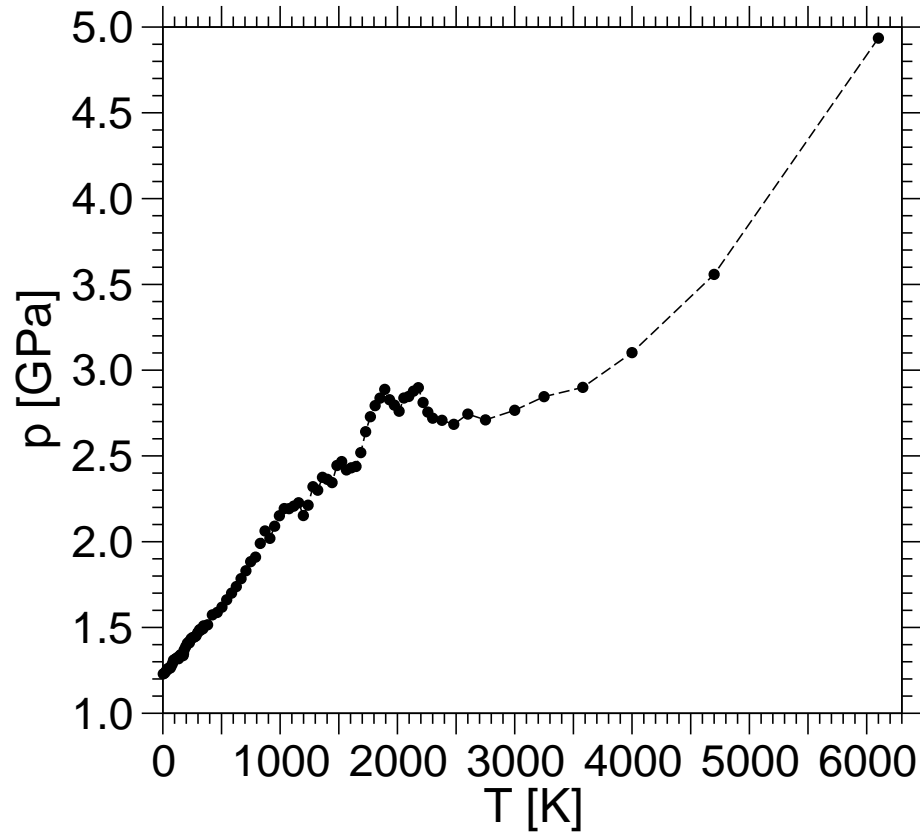


Figure 2: The pressure as a function of temperature. Note that the points for $T < 2300$ K are sampled during runs where the system was cooled down from 2300 K to 0 K with a cooling rate of $\gamma = 1.42 \cdot 10^{12}$ K/s.

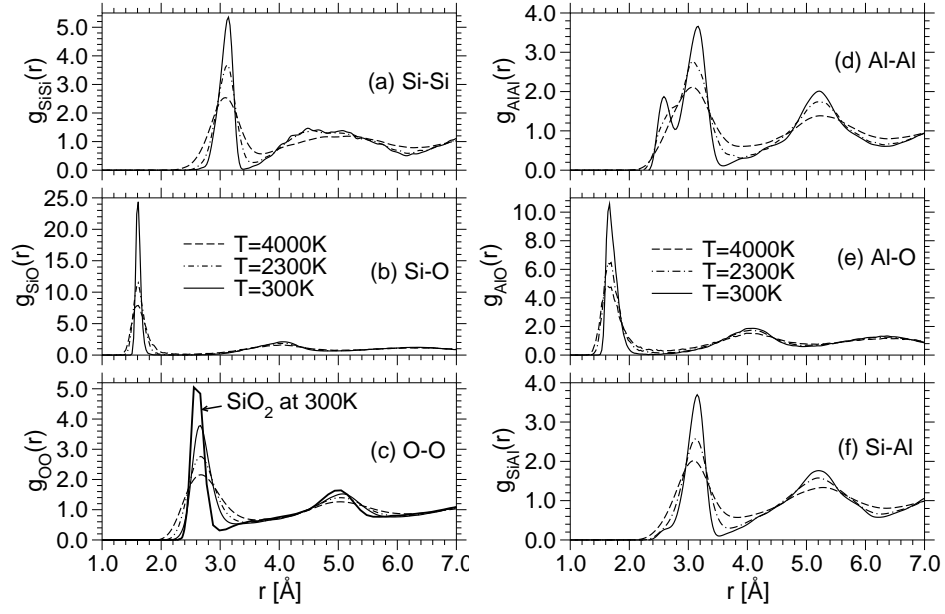


Figure 3: Partial pair correlation functions $g_{\alpha\beta}(r)$ for the temperatures $T = 4000\text{ K}$, 2300 K and 300 K . a) $g_{\text{SiSi}}(r)$, b) $g_{\text{SiO}}(r)$, c) $g_{\text{OO}}(r)$, d) $g_{\text{AlAl}}(r)$, e) $g_{\text{AlO}}(r)$, f) $g_{\text{SiAl}}(r)$. The curve in c) for SiO_2 at $T = 300\text{ K}$ is taken from Ref. [8].

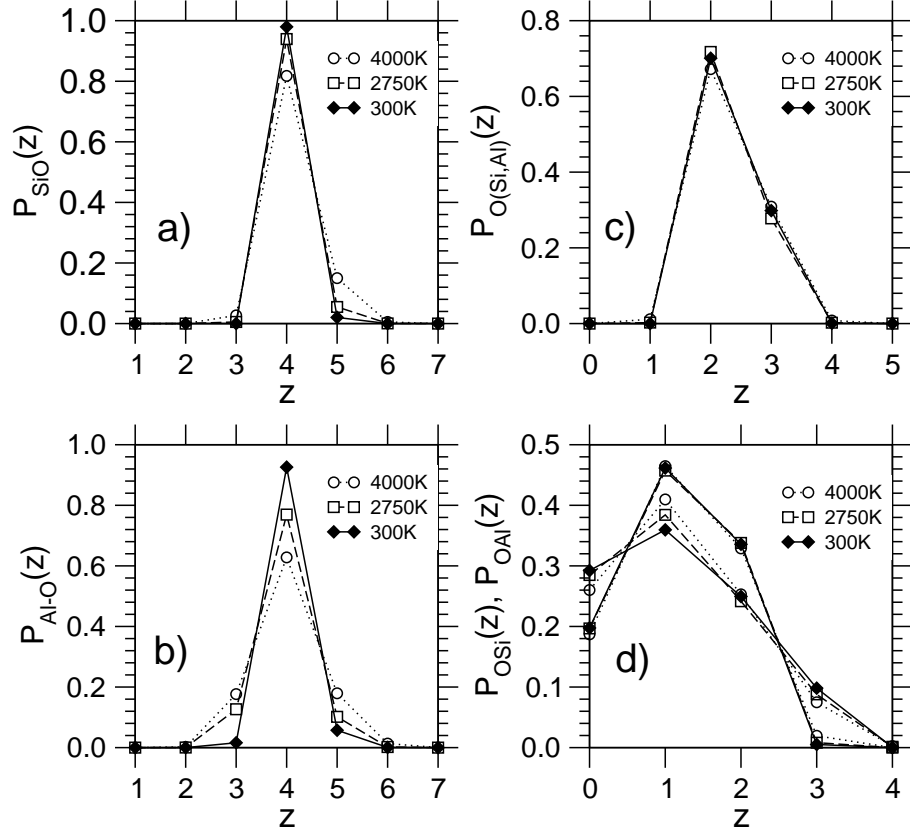


Figure 4: Distribution of coordination numbers $P_{\alpha\beta}(z)$ for the temperatures $T = 4000$ K, 2300 K and 300 K, a) $P_{\text{SiO}}(z)$, b) $P_{\text{AlO}}(z)$, c) $P_{\text{O}(\text{Si,Al})}(z)$, d) $P_{\text{OSi}}(z)$ and $P_{\text{OAl}}(z)$. The three curves that at $z = 2$ have the largest values correspond to $P_{\text{OSi}}(z)$.

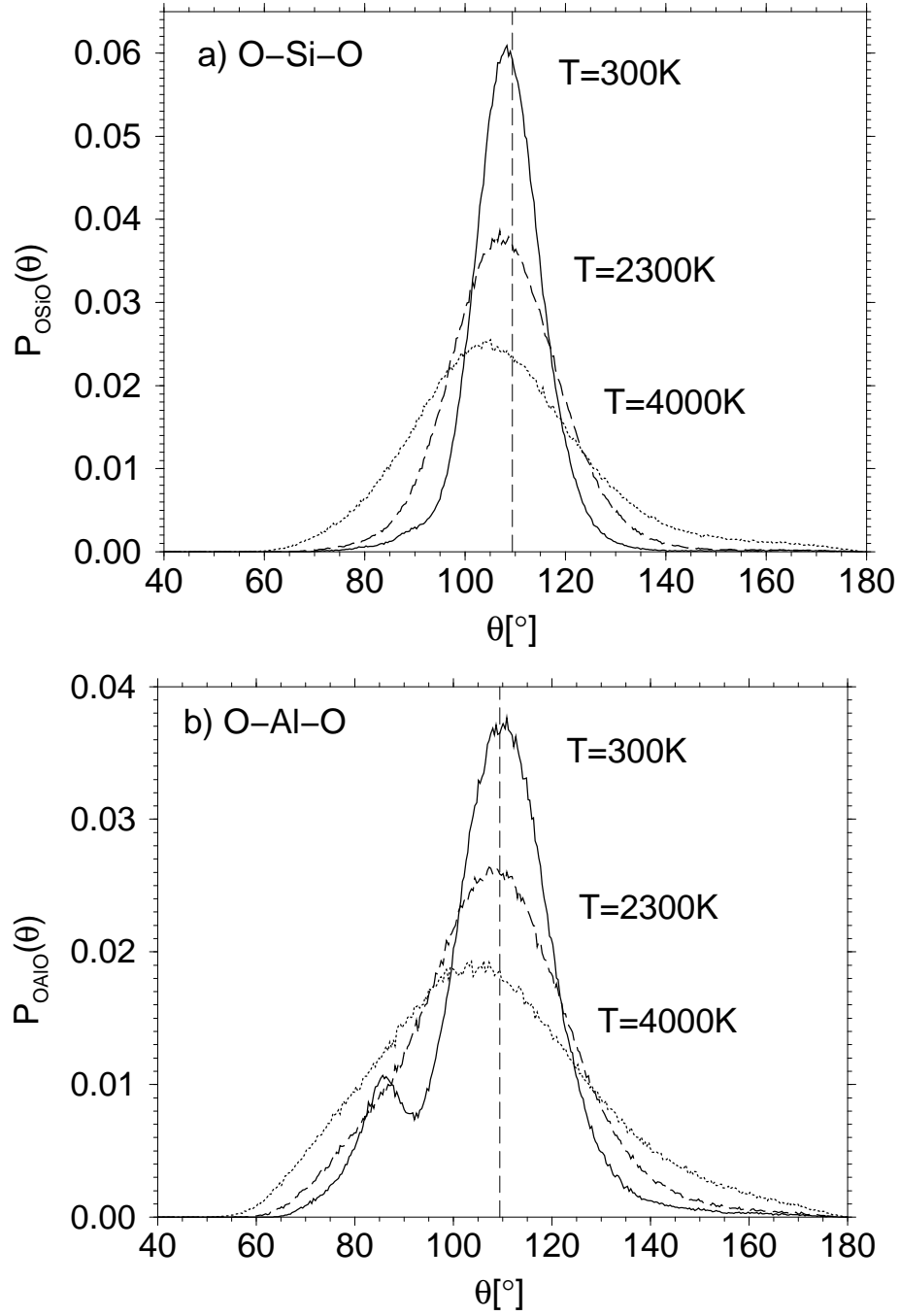


Figure 5: Distributions of angles θ for the temperatures $T = 4000\text{ K}$, 2300 K and 300 K , a) $P_{\text{OSiO}}(\theta)$, b) $P_{\text{OAlO}}(\theta)$. The vertical lines correspond to the ideal tetrahedron angle of 109.47° .

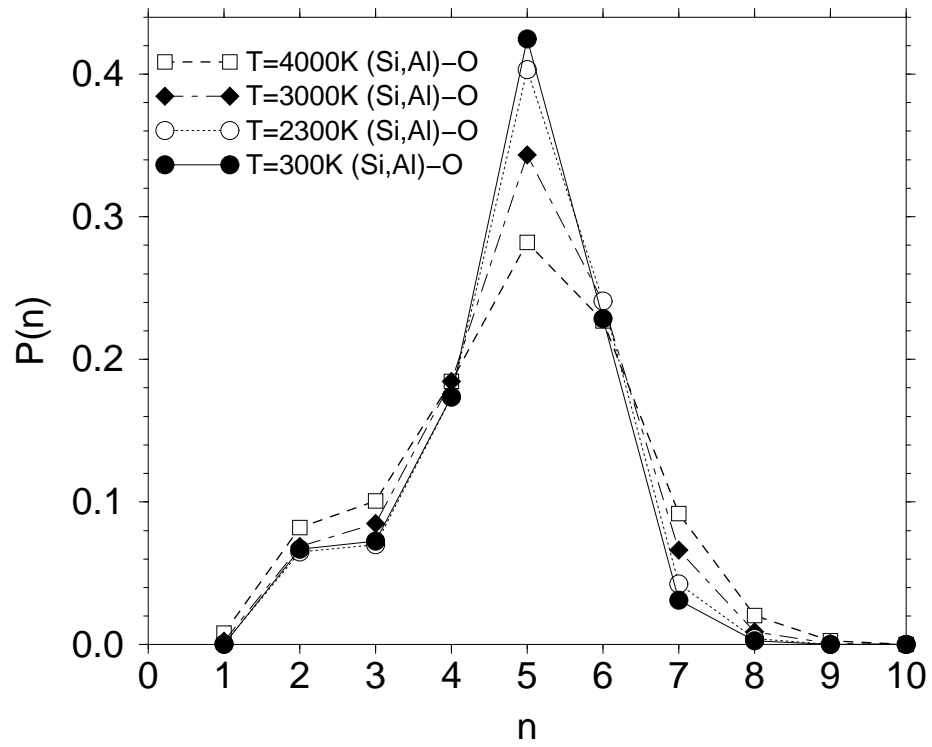


Figure 6: Distribution of rings $P(n)$ for the temperatures $T = 4000$ K, 3000 K, 2300 K and 300 K. See text for the definition of a ring.

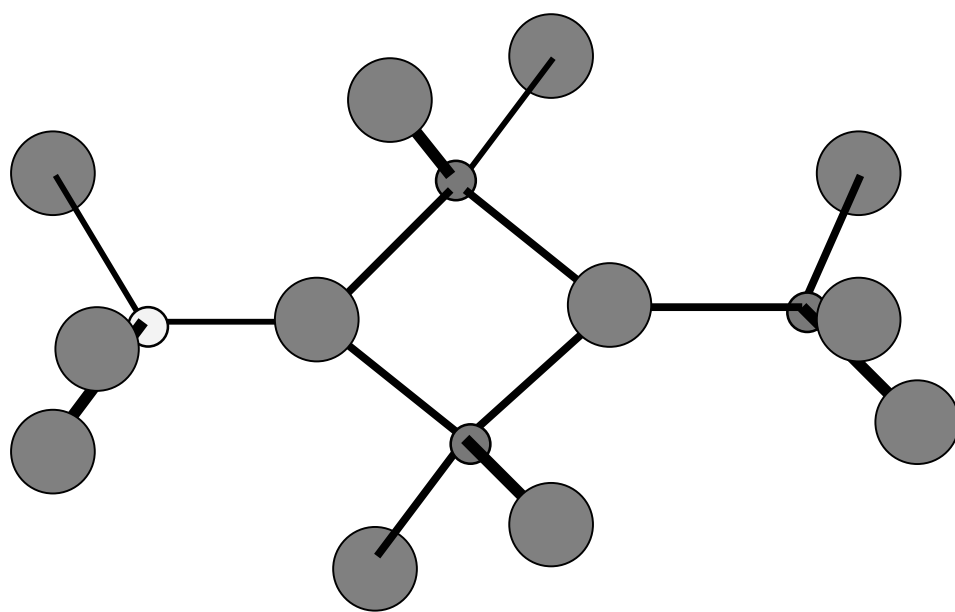


Figure 7: Schematic picture of a typical local configuration in AS₂. O atoms are the big grey spheres, Al atoms are the small grey spheres, and the light small sphere is a Si atom. The black lines between the atoms symbolize covalent Al–O and Si–O bonds. The picture shows a two-membered Al–O ring whereby the O atoms in this ring form triclusters.

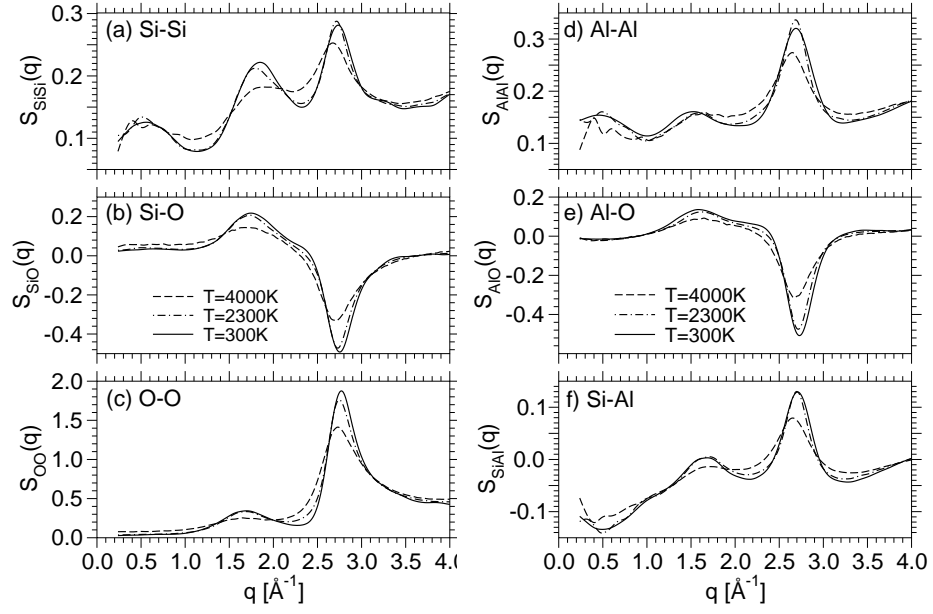


Figure 8: Partial static structure factors $S_{\alpha\beta}(q)$ for the temperatures $T = 4000$ K, 2300 K and 300 K. a) $S_{\text{SiSi}}(q)$, b) $S_{\text{SiO}}(q)$, c) $S_{\text{OO}}(q)$, d) $S_{\text{AlAl}}(q)$, e) $S_{\text{AlO}}(q)$, f) $S_{\text{SiAl}}(q)$.

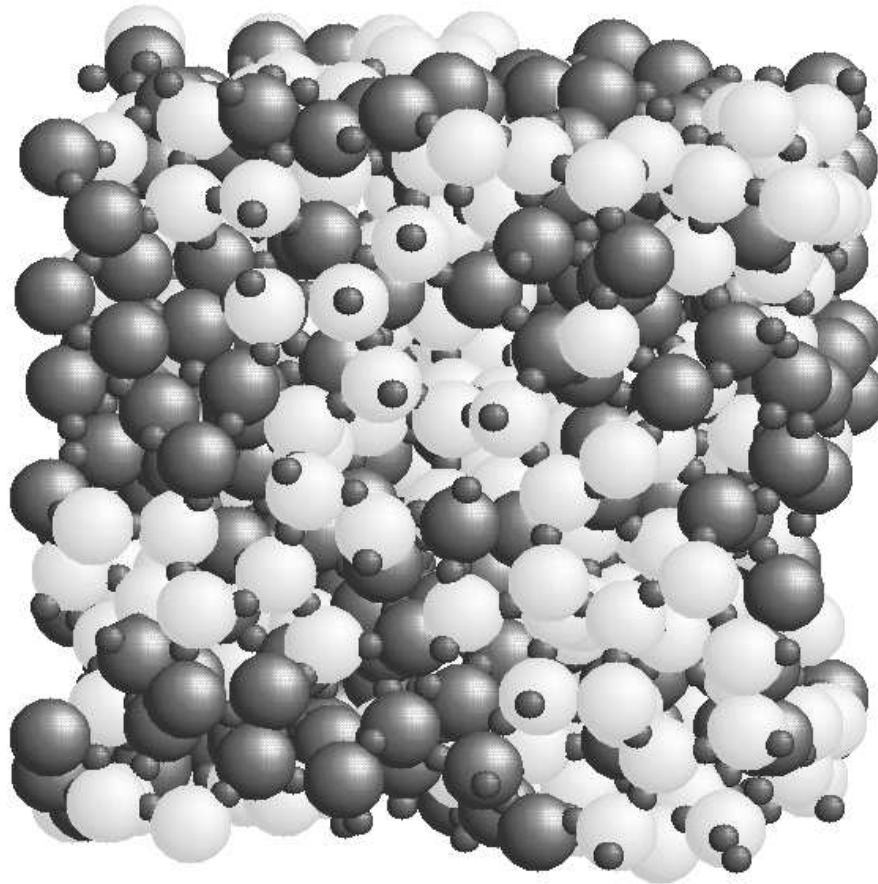


Figure 9: Snapshot of AS2 at $T = 300$ K. The big white spheres are the silicon atoms, the big black spheres are the aluminium atoms and the small black spheres are the oxygen atoms. Note that the size of the spheres does not correspond to the actual size of the atoms.

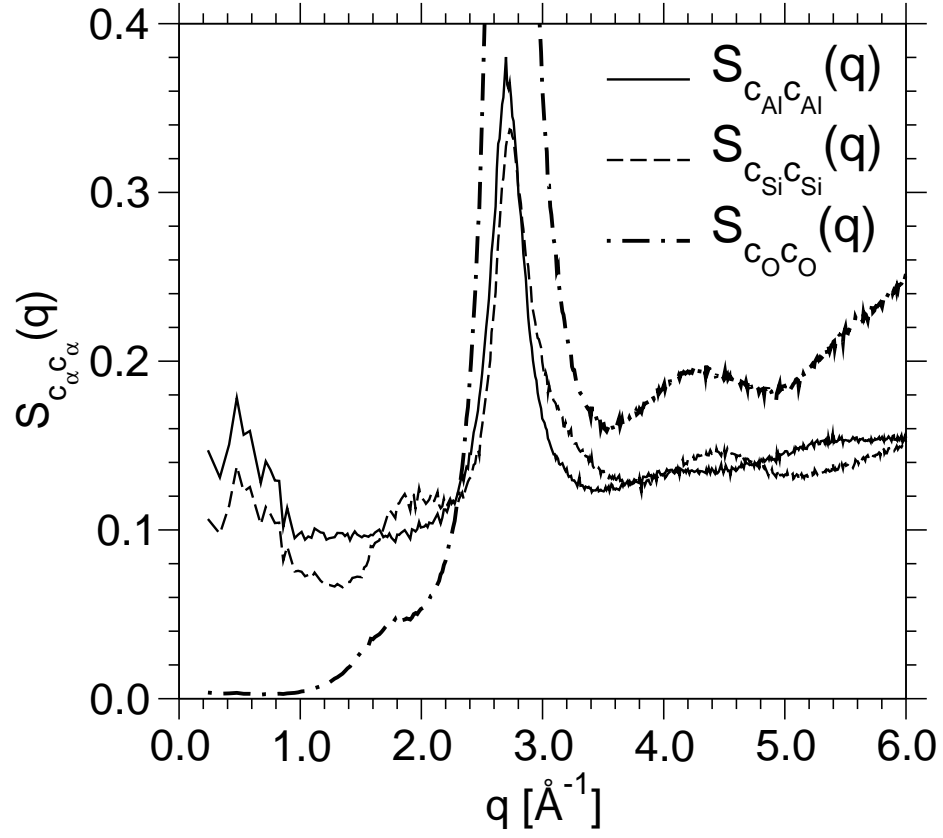


Figure 10: Structure factors $S_{c_{\alpha}c_{\alpha}}(q)$ ($\alpha \in [\text{Si}, \text{Al}, \text{O}]$) at $T = 2300$ K. See Eq. (9) for the definition of $S_{c_{\alpha}c_{\alpha}}(q)$.

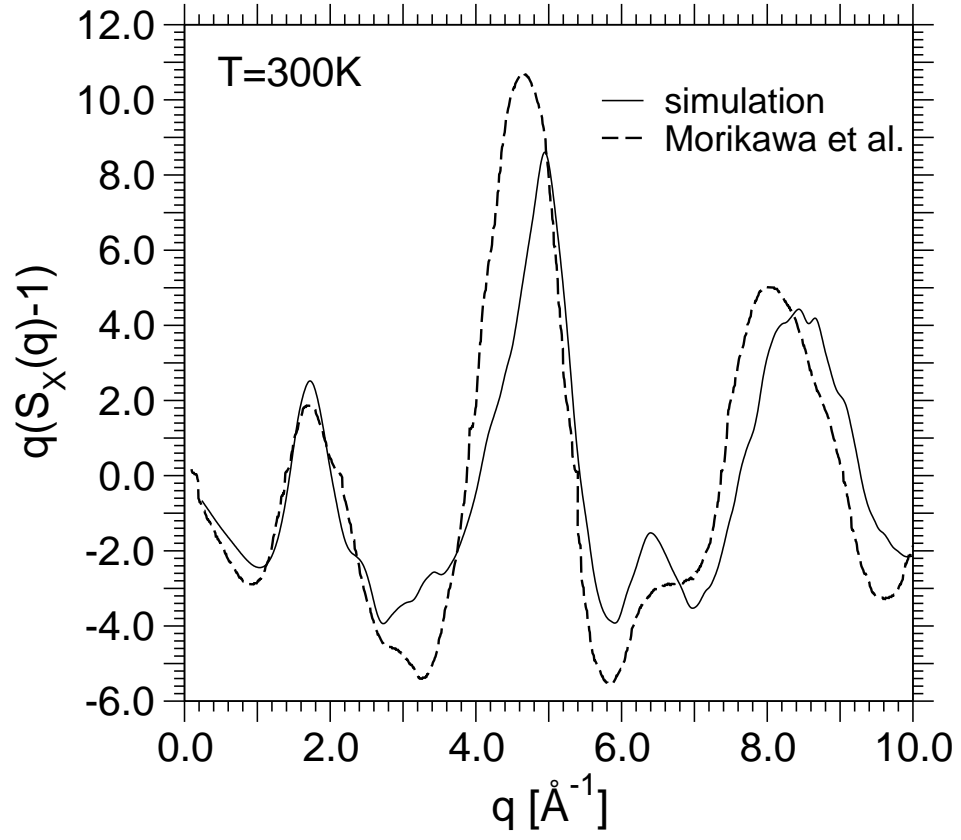


Figure 11: “Reduced” X-ray scattering factor $q(S_X(q) - 1)$ as calculated from the simulation using Eq. (10) (solid line) in comparison to the experimental result by Morikawa *et al.* [24] (dashed line).

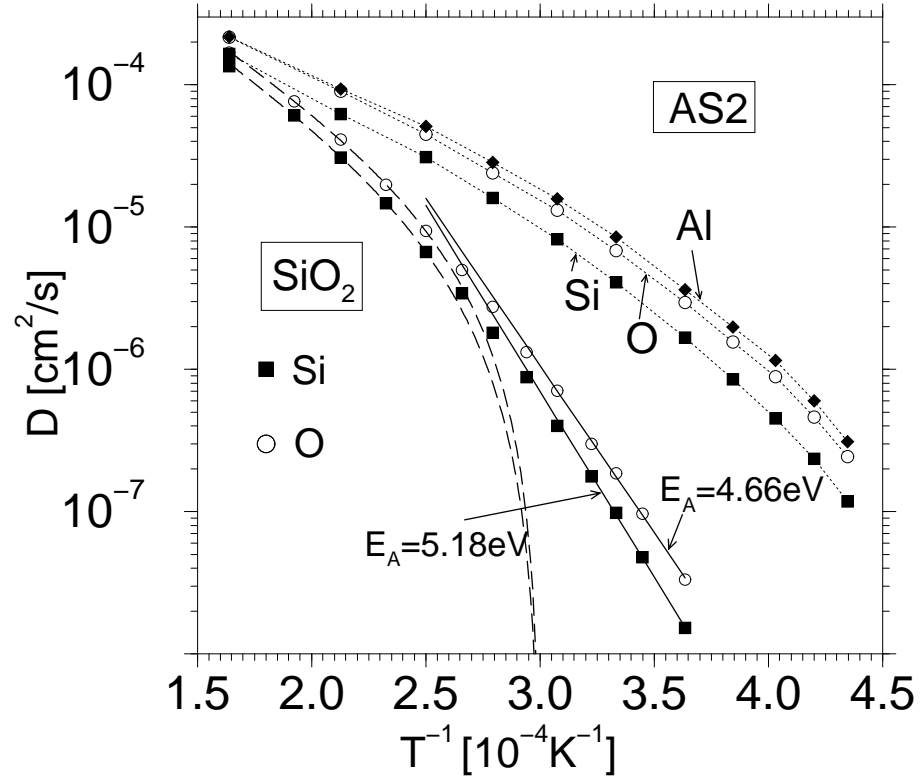


Figure 12: Arrhenius-plot of the diffusion constants of silicon, aluminium and oxygen: Comparison of the systems AS2 and SiO_2 (the data for SiO_2 is taken from Ref. [8]). The dashed lines are power law fits to the SiO_2 data (see text for details).

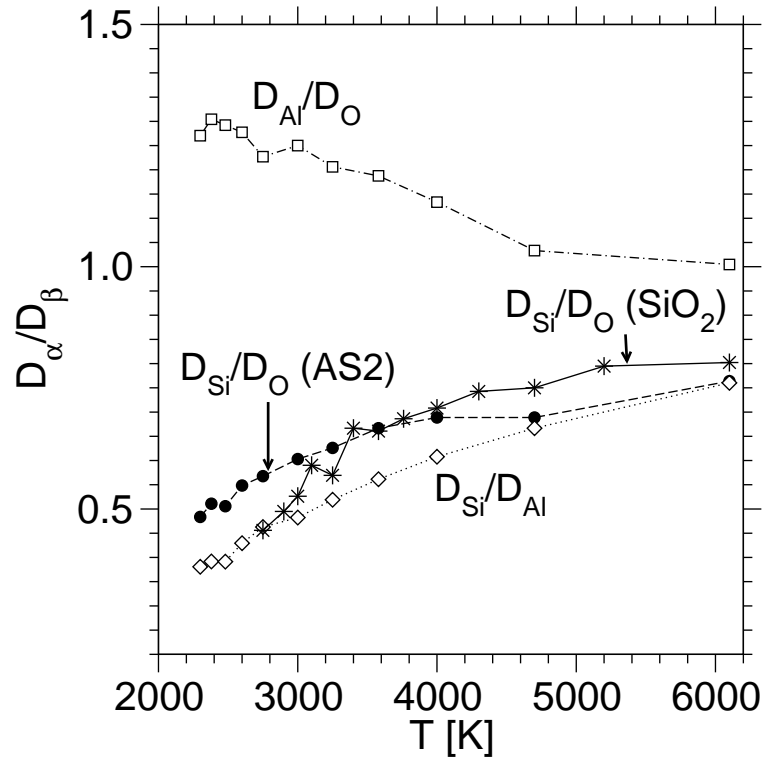


Figure 13: Temperature dependence of the indicated ratios of the diffusion constants D_α/D_β ($\alpha, \beta \in \{\text{Si}, \text{Al}, \text{O}\}$).